Three-dimensional visualization of viscous fingering for non-Newtonian fluids with chemical reactions that change viscosity

Sotheavuth Sin,[1,*] Tetsuya Suekane,[1,†] Yuichiro Nagatsu,[2] and Anindityo Patmonoaji[1]
[1]*Department of Mechanical Engineering, Tokyo Institute of Technology, 2-12-1-I6-33, Ookayama, Meguro-ku, Tokyo, 152-8550, Japan*
[2]*Department of Chemical Engineering, Tokyo University of Agriculture and Technology, 2-24-16 Naka-cho, Koganei, Tokyo 184-8588, Japan*

(Received 31 October 2018; published 24 May 2019)

Viscous fingering (VF) is a hydrodynamic flow instability that occurs when a less-viscous liquid (LVL) displaces a more-viscous liquid (MVL) in porous media and takes place in either miscible or immiscible systems. In this study, we investigated the three-dimensional (3D) characteristics of VF for miscible non-Newtonian fluids with and without chemical reactions using a microfocus x-ray computed tomography scanner. When the viscosity of a system increased with a chemical reaction, the VF was suppressed, and pistonlike displacement occurred. The cylindrical domain of displacing LVL was surrounded by a high-viscosity filmlike layer because of the chemical reaction that impeded the mixing of the LVL and MVL. Consequently, the high LVL concentration inside this layer was retained without mixing with the MVL. A clear local peak in viscosity appeared in the viscosity profiles at the interface between the LVL and MVL. Behind the peak, an unfavorable viscosity profile of increasing viscosity along the flow direction appeared, but the VF was not induced because of the smooth viscosity gradients. After the peak, the viscosity profiles were in favorable conditions. In the nonreactive case, the tip of the fingers further advanced compared with that in the reactive case and went further with the decrease in Pe, which reflected the property of shear-thinning fluids. By contrast, in a decreasing-viscosity system with a chemical reaction, the tips of the fingers were located at a larger distance compared with that without reaction. The concentration in the finger intensively decreased from the point of injection because of the intensive mixing of the LVL and MVL. As a result, the area fraction of injected LVL in the reactive cases was lower than that in the nonreactive cases. The tip of the finger advanced with time, whereas LVL concentration in the finger hardly recovered above 0.4 in the reactive case, which reflected intensive fingering and mixing.

DOI: 10.1103/PhysRevFluids.4.054502

I. INTRODUCTION

Viscous flow instabilities that originate from the difference in viscosity and/or density have been intensively studied over the past few decades not only theoretically but also experimentally [1] owing to their diverse applications in many engineering fields such as petroleum recovery [1], hydrology [2], CO_2 sequestration [3,4], liquid crystal [5], chromatographic separation [6], and polymer processing [7]. Viscous fingering (VF) is a hydrodynamic flow instability that occurs when a more-viscous liquid (MVL) in a medium is driven forward by an injected less-viscous liquid

*sin.s.ab@m.titech.ac.jp
†tsuekane@es.titech.ac.jp

(LVL) both in miscible and immiscible systems [1,8–11]. When the density difference between the two fluids is negligible, VF is characterized by two dimensionless parameters. One is the viscosity ratio (M), which is defined as the ratio of the viscosity of the displaced fluid to that of the displacing fluid [12]. The other is the Péclet number (Pe) or capillary number (Ca), which characterizes the flow field of miscible and immiscible systems, respectively. Pe is defined as the ratio of the mass transport by advection to that by diffusion, whereas Ca is defined as the ratio of the viscous shear force to the interfacial tension. In the present study, we focused on the VF in a miscible system of non-Newtonian fluids with chemical reaction.

The VF formed in non-Newtonian fluid systems has received much attention because it displays an interestingly different and large variety of structures compared with that in Newtonian fluid systems [13]. The distinctive feature of the VF structures in non-Newtonian fluid systems, i.e., finger narrowing and finger widening, might be caused by the properties of the non-Newtonian fluids, such as shear-thinning or shear-thickening and elasticity effects. For flexible-polymer solutions, the two dominant parameters that influence the VF structures are elasticity and larger elongation viscosity. The elasticity effect is usually caused by normal stresses. For rigid-polymer solutions, however, shear viscosity is considered as the most influential parameter on the VF, whereas the elasticity effect is negligible [14–16]. For shear-thinning fluids, decreasing the power law index (shown later as n) dramatically increases the growth rates of perturbations to the interface and leads to greater tip splitting and hence to more ramified VF patterns [14,15,17,18]. The shear-thinning viscosity strikingly enhances the shielding effect, and the fingers form a branched structure [19].

A chemical reaction also dramatically changes the VF pattern because of the production of a surfactant [20–24], precipitation [25–27], or change in viscosity [9,28–39]. Nagatsu *et al.* [32] conducted an experimental study of miscible VF induced by a variation in viscosity in the presence of instantaneous chemical reactions. They explained that finger narrowing and enhancement of the shielding effect caused by the decrease in viscosity were due to the reactions. On the other hand, an increase in viscosity due to the reactions resulted in finger widening and suppression of the shielding effect. The similarity between a smaller viscosity at the tips of the advancing fingers induced by a high shear rate and that by the chemical reactions that caused finger narrowing was discussed [14,32]. Fernandez and Homsy [20] performed immiscible VF experiments using a radial Hele-Shaw cell accompanied by chemical reactions and found that the finger width increased as the chemical-reaction-decreasing interfacial tension continued. As a result, the reactive fingers tended to become wider than the nonreactive fingers. De Wit and Homsy [28,37] conducted numerical simulations to investigate the nonlinear interactions of chemical reactions that influenced miscible VF in porous media. Chemical reactions could possibly accelerate nonlinear phenomena such as tip splitting and maintained a sharp front between the MVL and LVL [28]. The formation of droplet mechanisms in which a solution disconnected from the bulk and invaded other solutions was caused by the coupling of the hydrodynamic and chemical-reaction phenomena [28].

Most investigations of a VF structure and its development have been conducted in two-dimensional porous media [24,40,41] or Hele-Shaw cells [5,7,9,13–17,19,20,25–27,31–34 36,38,42–44] because of the opaque nature of such media and the simplicity of both experimental and theoretical treatments. Recent rapid progress in noninvasive three-dimensional (3D) visualization techniques such as magnetic resonance imaging (MRI) and x-ray computed tomography (CT) allows us to achieve rapid and high-resolution imaging [45,46]. Because the conventional MRI uses echo signals emitted by protons, the signal intensity reflects the local concentration of water. The signal intensity of an x-ray CT shows that the x-ray attenuation coefficient is roughly proportional to the atom number. Rose and Britton reported 3D VF induced by a chemical reaction in porous media using MRI at low flow rates [47]. In our previous study [3], we successfully visualized a time-lapse 3D structure of VF in porous media using a microfocused x-ray CT scanner. In the present study, we utilize the same nondestructive technique [48], which allows us to obtain sequential contiguous images to construct the 3D geometries of VF as well as local information such as the concentration in a porous medium. In this manner, we investigate the 3D structure of VF for non-Newtonian fluids with and without chemical reactions in porous media and visualize

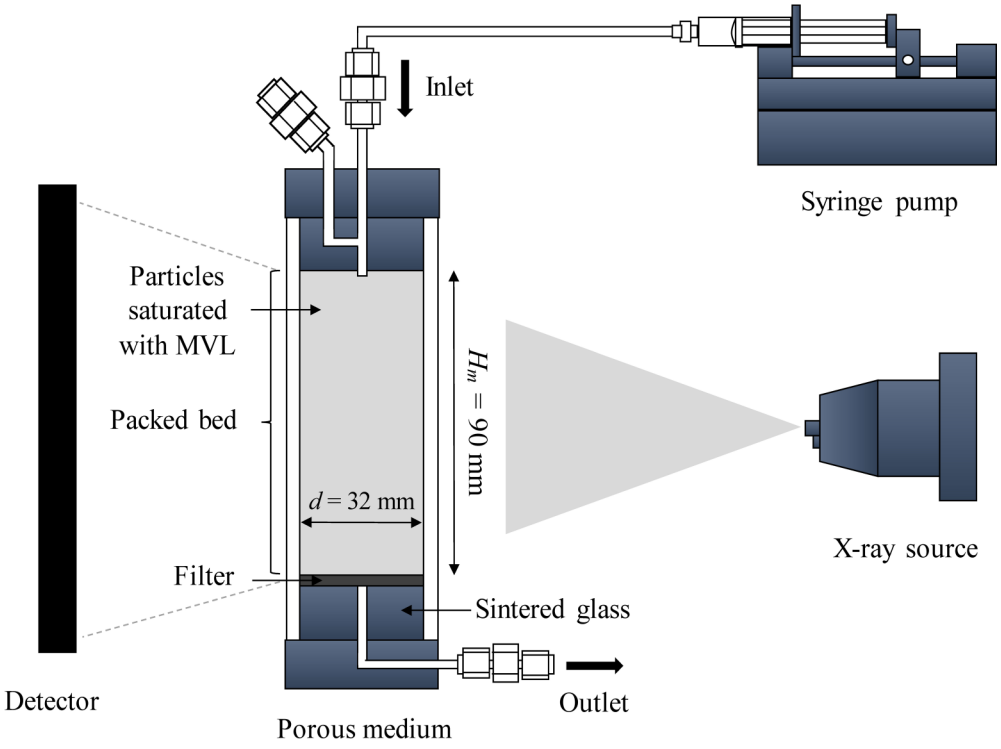

FIG. 1. Schematic of the experimental procedures.

the distribution of the concentration and viscosity of miscible VF. The next section presents the list of materials used in the current experiments and how the experimental works are performed. In Sec. III, the results of the present study are divided into two parts, namely, "Increasing-viscosity system," and "Decreasing-viscosity system," and are individually discussed. Each system composes the results such as the 3D structure of the fingers under different Pe conditions, changes in the displacing liquid concentration and viscosity, area fraction of the fingering, distribution of the maximum concentration and maximum viscosity along the fingers, and sweep efficiency. We finally present brief conclusions based on our present results.

II. MATERIALS AND METHODS

A packed bed of particles was used as a 3D porous medium. Melamine resin particles with diameters in the range $250 - 425\,\mu$m ($d_{50} = 337.5\,\mu$m, Ube Sand Engineering Co. Ltd.; XH series) were packed in a tube with inner diameter d of 32 mm over the height H_m of 90 mm, as shown in Fig. 1. A sintered glass filter plate was placed at the exit of the packed bed to facilitate uniform drainage. Patmonoaji and Suekane [49] investigated the dissolution of the capillary trapped gas bubbles in porous media via mass transfer using the same plastic particles and packed bed used in the current study. They used commercial software (ExFact VR 2.0 Nihon Visual Science; originally developed as 3DMA-Rock) to process the 3D images of the medium to determine the pore and throat size distributions of the particles. As a result, the average pore size was 1.32×10^{-3} mm^3 (300 voxels), which corresponded to a median effective pore diameter of $127.53\,\mu$m and a median effective throat diameter of $34.90\,\mu$m [49]. By measuring the change in the weight of the porous medium before and after saturation with water, porosity φ was estimated to be 0.47, whereas permeability k determined from water flooding was 2.34×10^{-10} m^2.

TABLE I. Properties of MVL and LVL.

Type	Fluids	Compositions	Density, ρ (kg/m^3)	Viscosity, μ (mPa s)
Displaced liquid or more-viscous liquid (MVL)	PAA	0.95 wt % Polyacrylic acid + 5 wt % sucrose	1000.70	[a]
	SPA	0.5 wt % PAA + 5 wt % sucrose + 0.1 *M* NaOH	1000.78	[a]
Displacing liquid or less-viscous liquid (LVL)	NaI	3 wt % NaI	1000.48	0.88[b]
	NaOH	3 wt % NaI + 0.1 *M* NaOH	1001.20	0.90[b]
	HCl	3 wt % NaI + 0.1 *M* HCl	1000.36	0.86[b]

[a]Viscosity of polymer solutions (PAA and SPA) changes with shear rate.
[b]Viscosity of Newtonian fluids (NaI, NaOH, and HCl) is constant with shear rate.

Nagatsu *et al.* [32] employed the dependence of the viscosity of polyacrylic acid (PAA) and sodium polyacrylate (SPA) solutions on *p*H. In the present study, we employ the same fluids as non-Newtonian fluids in which the viscosity changes with the chemical reaction. When the PAA solution is displaced by a sodium hydroxide (NaOH) solution, the chemical reaction produces SPA in the mixture, increasing the viscosity with *p*H [32]. On the other hand, when the SPA solution is displaced by a hydrochloric acid (HCl) solution, the viscosity of the mixture reduces with the chemical reaction [32]. In the current study, we employ two chemically reactive fluid pairs of a PAA-NaOH system with an increasing viscosity and an SPA-HCl system with decreasing viscosity. For reference, NaI solutions are used, instead of NaOH and HCl solutions, respectively, for the nonreactive system. Table I lists a summary of the properties of the fluids used in the present experiments. We use PAA whose molecular weight is 1 000 000 (Wako, Japan), whereas SPA was produced by mixing PAA and NaOH via chemical reaction [9,32,33]. To match the density between the MVL and the LVL, we add a sucrose solution to the MVL to exclude the effect of gravitational force. We add 3 wt % of NaI into the LVL because of the high x-ray attenuation of NaI. The local concentration of LVL is evaluated using the CT value in the calibration curve obtained from preliminary experiments (Fig. 1 in the Supplemental Material [50]).

We performed the experiments using the following procedures. First, the packed bed of plastic particles was saturated with MVL using a vacuum chamber. We then vertically placed it in the x-ray CT scanner (Comscantechno, ScanXmate-RB090SS) between the x-ray source and detector (Varian, PaxScan 1313DX) for the first scan to confirm that no trapped gas bubbles were present in the packed bed. Second, the MVL that remained in the injection tubing at the top part of the porous medium was replaced by injecting air, followed by LVL through a bypass line to prevent a chemical reaction in the injection tubing. Third, we injected the LVL vertically downward with respect to the direction of gravitational acceleration into the packed bed with a constant flow rate using a syringe pump (KD Scientific, KDS100).

The Péclet number (Pe), which is a dimensionless number that controls the fingering, is expressed as

$$\mathrm{Pe} = \frac{\mathrm{vd}}{\mathrm{D_m}}, \tag{1}$$

where $v = Q/(\varphi A)$ is the interstitial velocity, Q is the volumetric flow rate of the injected LVL, A is the cross-sectional area of the packed bed, and $\mathrm{D_m}$ is the diffusion coefficient between the MVL and LVL, estimated to be 1.0×10^{-9} m^2/s, which is the diffusion coefficient of the polymer with a small concentration in water [32].

TABLE II. Experimental conditions.

System	Fluids	Pe	$\dot{\gamma}$ (1/s)	μ_{MVL} (mPa s)	M
Increasing viscosity	PAA-NaOH (reactive)	1.42×10^2	1.01	408	452
		1.42×10^3	10.1	157	174
		2.84×10^3	20.2	118	130
		5.68×10^3	40.4	88.6	98.0
	PAA-NaI (nonreactive)	1.42×10^2	1.01	408	460
		1.42×10^3	10.1	157	177
		2.84×10^3	20.2	118	132
		5.68×10^3	40.4	88.6	99.8
Decreasing viscosity	SPA-HCl (reactive)	0.71×10^2	0.50	2240	2608
		1.42×10^3	10.1	511	596
		2.84×10^3	20.2	365	425
		5.68×10^3	40.4	261	304
	SPA-NaI (nonreactive)	0.71×10^2	0.50	2240	2522
		1.42×10^3	10.1	511	576
		2.84×10^3	20.2	365	411
		5.68×10^3	40.4	261	294

The viscosity of non-Newtonian fluids depends on shear rate, $\dot{\gamma}$. We can reasonably estimate the shear rate using the analogy of the flow of Newtonian fluids in a pipe as follows:

$$\dot{\gamma} = \frac{\mathrm{v}}{\frac{\mathrm{d_{th}}}{8}}, \tag{2}$$

where d_{th} is the median effective throat diameter among the pores.

Table II lists a summary of the experimental conditions in each pair of fluids. In the present experiments, Pe was varied in the range of $0.71\times10^2 \leqslant \mathrm{Pe} \leqslant 5.68\times10^3$ corresponding to a range of shear rate from $0.50 \leqslant \dot{\gamma} \leqslant 40.44\,\mathrm{s}^{-1}$. For a low-flow-rate condition ($\mathrm{Pe} = 0.71\times10^2$), we injected each with 0.005 pore volume (PV) of the LVL in the SPA-HCl and SPA-NaI cases into the packed bed and performed continuous scanning until breakthrough when the LVL reached the exit of the packed bed because the migration of fluid during the scan (approximately 80 s) was negligible. For the PAA-NaOH and PAA-NaI cases, however, we followed the same procedures, but the amount of LVL injected into the packed bed was 0.01 PV with $\mathrm{Pe} = 1.42\times10^2$. For the high-flow-rate conditions ($1.42\times10^3 \leqslant \mathrm{Pe} \leqslant 5.68\times10^3$), we stopped the injection and scanned the packed bed after 0.05 PV of LVL was injected to prevent the migration of fluid during the scan. Each experiment was performed and finished within 3 h. In addition, in every experiment, the porous medium was packed with new plastic particles. Therefore, the swelling of particles due to absorption or adsorption of liquid solutions (acid or alkali) that change the properties of porous media, i.e., porosity and permeability, was negligible.

An x-ray microfocus CT scanner was used to visualize the 3D VF that occurred inside the packed bed. In each scan, the packed bed rotated by 360° between the x-ray source and detector to obtain 625 images from all directions at 8.0 frames per second. Therefore, a single scan took approximately 80 s. To eliminate the drift in brightness of the CT value among the scans, the x-ray scanner was operated with a constant voltage of 90 kV and current of 90 μA of the x-ray source in each scan. The reconstructed images consisted of $992 \times 992 \times 992$ pixels with a pixel size of 103 μm/pixel along the entire volume of the packed bed. In this reconstruction process, additional filters installed in the reconstruction software of the x-ray CT scanner were applied to eliminate noise, ring artifact, and the beam-hardening effect. The CT value was adjusted so that the CT values of the acrylic resin tube of the packed bed and surrounding air were the same for all scans. Then, the images were subtracted by the first scan image taken before the LVL injection by using the IMAGE CALCULATOR of the image-processing software (IMAGEJ). This image subtraction allowed us to enhance the change

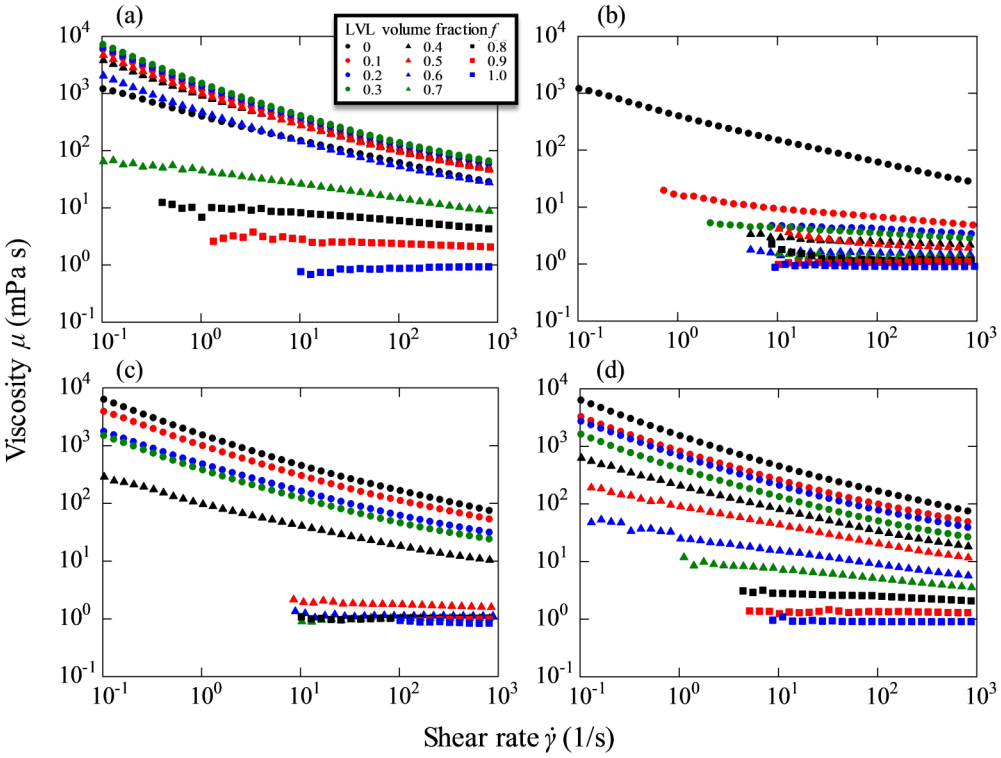

FIG. 2. Dependence of the viscosity of the mixtures of (a) PAA-NaOH, (b) PAA-NaI, (c) SPA-HCl, and (d) SPA-NaI on the shear rate under various volume fractions.

in the CT value and remove local bright spots associated with the metal impurities contained in the particles because of the higher degree of reproducibility of the positions of the 3D images. We finally transformed the local gray values to local concentrations based on the calibrated curves (Fig. 1 in the Supplemental Material [50]) obtained from the initial experiments.

The viscosity of the polymer solutions was measured using a rotational rheometer (ARES-G2, TA Instruments) by changing the volume fraction of the LVL and MVL mixture. Because polymer solutions are generally non-Newtonian fluids, they show two dominant non-Newtonian characteristics, namely, shear rate and elasticity. In the present study, the elasticity was negligible because no measurable normal stress was present in the shear rate range of $\dot{\gamma} \leqslant 10^3\ \mathrm{s}^{-1}$ for the PAA and SPA solutions [32]. Figure 2 shows the viscosity measurement results of all liquid combinations used in the present study. The PAA and SPA solutions (LVL volume fraction $f = 0$) clearly exhibited the characteristic property of the shear-thinning fluid, where the viscosity of the solutions decreased with the increase in shear rate, $\dot{\gamma}$. The NaOH, HCl, and NaI solutions (LVL volume fraction $f = 1$) displayed a Newtonian fluid property where the viscosity was constant for the shear rate. The viscosity of the mixtures showed a gradual transition from a shear-shinning fluid to a Newtonian fluid with the increase in the LVL volume fraction. Reliable viscosity was not available at low shear rates because of the rheometer limitation. The Ostwald–de Waele power law model, i.e., $\mu = k\dot{\gamma}^{n-1}$ [14,32] was fitted to the data points shown in Fig. 2 to estimate the values of k and n ($0 \leqslant n \leqslant 1$) (Table I in the Supplemental Material [50]). The power law model was extrapolated to estimate the viscosity at low shear rates.

Figure 3 shows the dependence of the viscosity of the mixtures on the LVL volume fraction for various shear rates. For the nonreactive case [Fig. 3(b), PAA-NaI], the viscosity of the polymer solution sharply decreased with the increase in the LVL volume fraction, and the shear-thinning

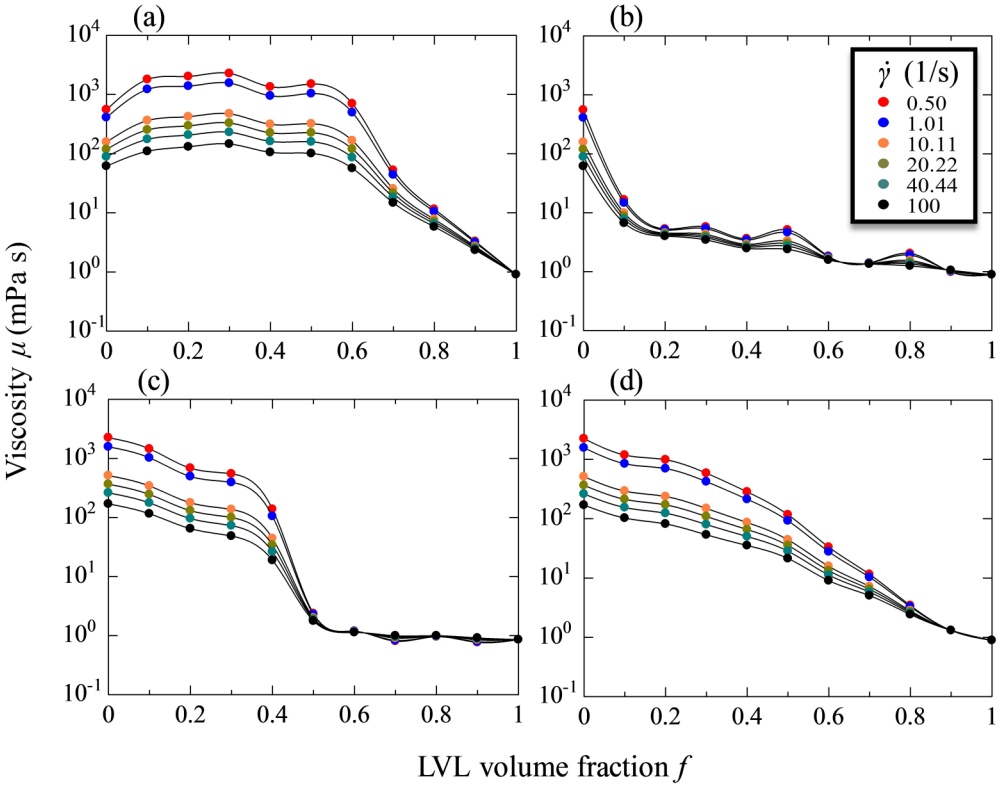

FIG. 3. Dependence of the viscosity of the solutions of (a) PAA-NaOH, (b) PAA-NaI, (c) SPA-HCl, and (d) SPA-NaI on the LVL volume fraction under various shear rates.

property was lost. However, for the reactive case [Fig. 3(a)], because of the instantaneous chemical reaction, the viscosity of the PAA-NaOH solutions increased for the LVL volume fraction range between 0.1 and 0.6 and then remarkably decreased with the LVL volume fraction. On the other hand, the viscosity of the SPA-HCl solutions [Fig. 3(c)] decreased with increasing LVL volume fraction, and a steep decrease in viscosity could be observed at $f = 0.4$ to 0.5. The solutions possessed a shear-thinning property for an LVL volume fraction lower than 0.4, whereas the solutions transformed to a Newtonian fluid for an LVL volume fraction higher than 0.5. For the nonreactive case of the SPA-NaI system [Fig. 3(d)], the viscosity monotonically decreased with the increase in the LVL volume fraction, and the shear-thinning property reduced at $f = 0.9$. In the nonreactive system, the retention of the properties of a polymer solution such as shear-thinning fluids for higher f values could be attributed to the MVL in the SPA-NaI system, which is one order of magnitude higher than that in the PAA-NaI system.

III. RESULTS AND DISCUSSIONS

A. Increasing-viscosity system

In this section, we present the experimental results of the PAA-NaOH system, where the chemical reaction increases the viscosity of the mixture using the PAA-NaI solutions without a chemical reaction as the reference system.

1. Effect of the Péclet number (Pe) on fingering

Figure 4 shows the 3D structure of the VF with and without viscosity increase in the chemical reaction after the injection of 0.05 PV of LVL into the packed bed saturated with MVL. All fingers

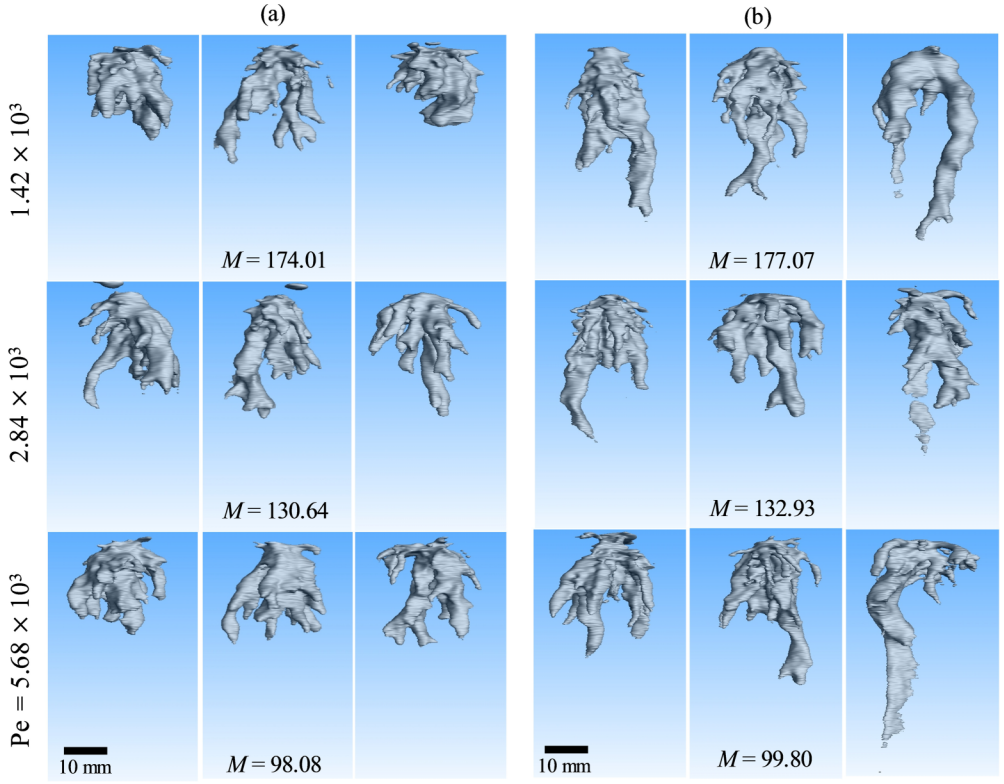

FIG. 4. 3D VF structure in the packed bed after injection of 0.05 PV of LVL for various Pe and M for the (a) reactive (PAA-NaOH) and (b) nonreactive (PAA-NaI) fluid pairs. The isocontour surface corresponds to the LVL concentration $f = C/C_0 = 0.25$. The three panels given for each M and Pe represent the results from three repeated experiments with the same experimental conditions.

are displayed as an isocontour surface at a normalized NaI concentration of $C/C_0 = 0.25$, which is equal to LVL volume fraction f. Hereafter, we consider the normalized NaI concentration to be equal to the LVL volume fraction $f = C/C_0$. For the reactive and nonreactive fluid pairs, LVL was injected at the same flow rate, i.e., Pe. The viscosity ratio was estimated from the LVL and MVL viscosities at the corresponding shear rates. It should be noted that a difference in viscosity ratio between the reactive and nonreactive cases at the same Pe was attributed to the difference in the viscosity of the NaOH and NaI solutions. For both reactive and nonreactive cases, VF was induced around the spot-injection point, and the fingers extended downward. In the reactive fluid case, the length of the fingers was shorter than that in the nonreactive fluid case where several long and thick fingers developed. It can be considered that the volume of the fingers in an isocontour surface tends to be large if the mixing of the LVL and MVL is significant. The finger volume in the reactive cases was lower than that in the nonreactive cases, which indicated that the LVL and MVL mixture was restrained by a chemical reaction. The diameter of the fingers was one or two orders of magnitude larger than that of the particles, which suggested that the VF observed in the present study developed in the Darcy scale [3].

2. Growth of fingers and distribution of local concentration and viscosity

Figures 5 and 6 depict the evolution of the 3D VF and distribution of the NaI concentration and viscosity with and without chemical reactions with the injection of every 0.01 PV at Pe = 1.42×10^2. The LVL concentration was estimated from the CT values in the correlation curves

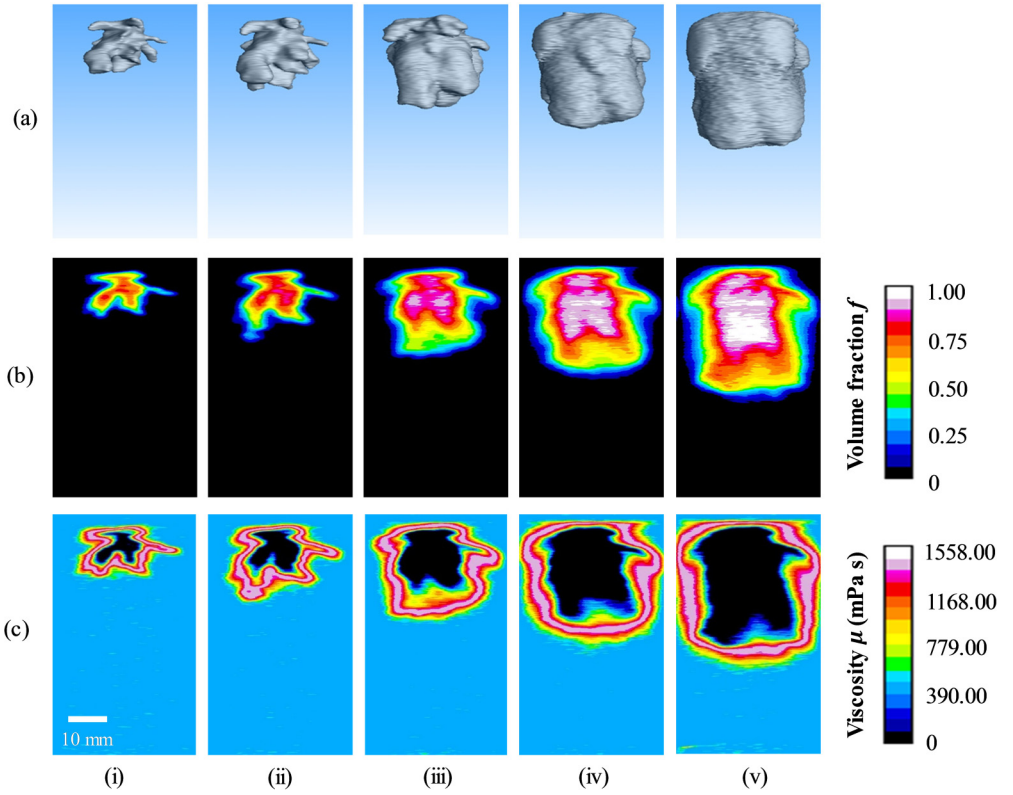

FIG. 5. Evolution of (a) 3D structure of the fingers, (b) LVL concentration, and (c) viscosity with chemical reaction (PAA-NaOH) at Pe $= 1.42 \times 10^2$ and $M = 452.46$ after injection of LVL (i) 0.02, (ii) 0.04, (iii) 0.10, (iv) 0.20, and (v) 0.30 PV.

obtained from the preliminary experiments (Fig. 1 in the Supplemental Material [50]). Then, the NaI concentration was transformed into the viscosity with curves, as shown in Fig. 3 (see Figs. 2–5 in the Supplemental Material for the detailed fitting curves [50]). Immediately after the injection started, VF appeared around the point of injection, but the fingers did not further grow in the reactive case (Fig. 5). Except for the region near the tube wall, pistonlike displacement took place in the packed bed. Immediately after the injection started, because a displacement front developed with a hemispherical shape centered at the point of injection, VF could develop. The finger tips were influenced by the tube wall; however, the fingers merged with one another, and a thick viscous layer was formed, which surrounded the LVL. The cylindrical domain of the displacing LVL was surrounded by a low-concentration ($f = 0.1 - 0.5$) filmlike layer, as shown in Fig. 5(b), where the viscosity was higher than 1000 mPa s because of the chemical reaction [Fig. 5(c)]. This viscous layer appeared to impede mixing of the LVL and MVL. Consequently, inside this layer, a high concentration of LVL was maintained without mixing with MVL. As a result, the fingering development was impeded, and the breakthrough was delayed. In a Hele-Shaw cell [32], a VF structure was observed over a wide range of Pe. The difference on whether VF occurred or not in the Hele-Shaw cell in the present experiments could depend on the flow configuration of a radial flow or flow in a constant area, respectively. For higher Pe shown in Fig. 4(a), LVL injection was stopped at 0.05 PV, which was close to 0.04 PV shown in Fig. 5(ii). In this study, injection of much more LVL did not perform for higher Pe. However, knowing whether the chemical reaction suppressed the VF or the instability at high Pe overcame the stabilization by chemical reaction

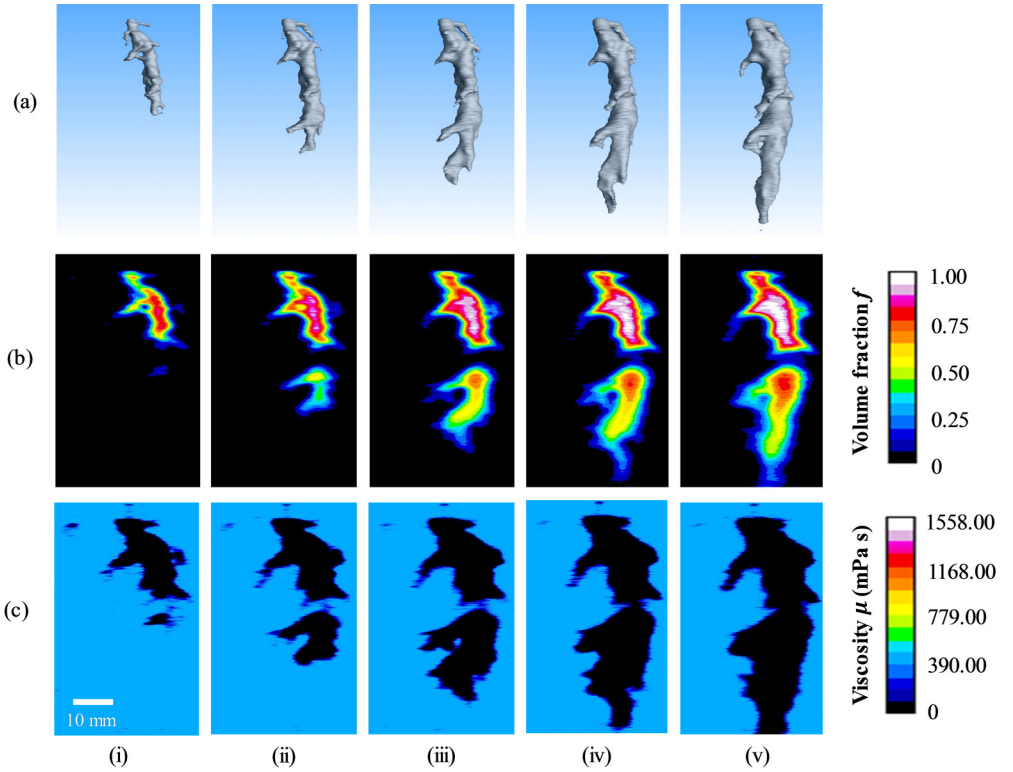

FIG. 6. Evolution of the (a) 3D structure of fingers, (b) LVL concentration, and (c) viscosity without chemical reaction (PAA-NaI) at Pe $= 1.42 \times 10^2$ and $M = 460.40$ after injection of LVL (i) 0.01, (ii) 0.02, (iii) 0.03, (iv) 0.04, and (v) 0.05 PV.

would be interesting. Daccord *et al.* [17] have shown that the pressure gradient in a radial Hele-Shaw cell tends to be uniform with the increase in $m = 1/n$. In the present study, the pressure gradient changed in the radial direction around the injection point because $n > 0.5$. In the nonreactive case, on the other hand, VF intensively developed because of a high viscosity ratio ($M = 460.40$) at a low shear rate (Fig. 6). Intensive VF resulted in the earlier breakthrough [Fig. 6(v)] with the injection of 0.05 PV of LVL. These results were consistent with the experimental and theoretical research works of shear-thinning fluids in a Hele-Shaw cell [14,15,18]. The concentration in the fingers decreased along the finger to its tip. Fig. 6(c) shows that intensive mixing of the LVL and MVL was induced around the fingers.

3. Area fraction of injected LVL

As shown in Fig. 4, three repeated experiments for each Pe and M were performed to investigate how the structure of the fingering pattern changes in the same conditions from one experiment to the other. We define the finger when the concentration of LVL is higher than $f = 0.25$. Figure 7 illustrates the area fraction of the LVL to the cross-sectional area of the packed bed. The distance from the injection point x is normalized by the height of the packed bed H_m. As a result, a similar trend of the area fraction profiles in the reactive and nonreactive case of each repeated experiment under the same Pe was clearly seen in Figs. 7(a) and 7(b), respectively. This suggested that even viscous fingering has extreme fluctuations from experiment to experiment; the repeatability of experiments under the same conditions would give a similar tendency of the fingering structure. In the case of the reactive fluid pair, the area fraction profiles resembled one another for all Pe

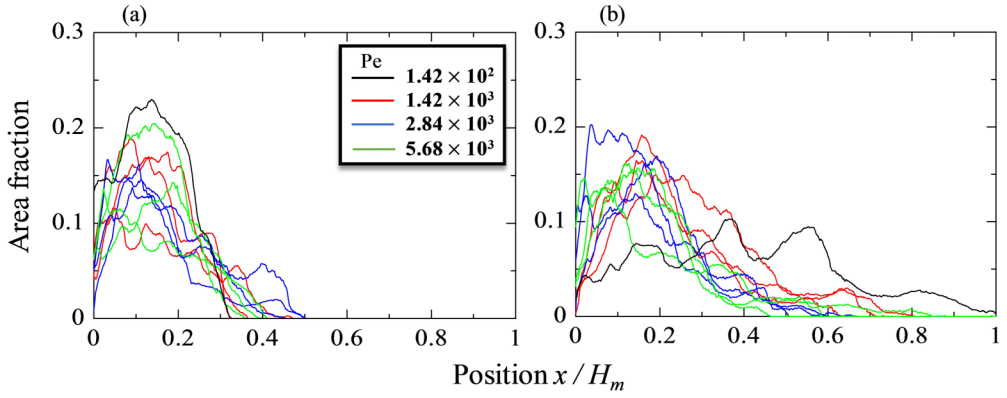

FIG. 7. Area fraction of LVL for various Pe values after injection of 0.05 PV of LVL for the (a) reactive (PAA-NaOH) and (b) nonreactive (PAA-NaI) fluid systems.

values, and the effects of Pe and M were not clear because of the suppression of VF due to the increase in the viscosity. In the nonreactive case, the tips of the fingers further advanced compared with that in the reactive case. The amount of injected LVL was 0.05 PV. Therefore, the large area below the lines shown in Fig. 7 indicated intensive mixing of the LVL and MVL. We can clearly see that the mixing was suppressed by a chemical reaction compared with that in the nonreactive cases. In the nonreactive fluid case with reduced Pe, namely, with increase in M, which reflected the property of shear-thinning fluids, the tip of the finger advanced much further.

4. Distribution of LVL concentration and viscosity along the most advanced fingering

Figure 8 shows the distribution of the maximum LVL concentration ($C_{\max}$) normalized with the initial concentration (C_0) along the most advanced finger for various Pe values. The maximum concentration in the most advanced finger for each horizontal cross-sectional area was obtained using the plug-in code FIND MAXIMA of the image-processing freeware (IMAGEJ). For high Pe values, the maximum LVL concentration in the reactive case linearly decreased from the injection port ($x/H_m = 0$) to the tips of the fingers, $x/H_m = 0.3$ to 0.6, and then sharply decreased at the tips. Figure 9 shows the distributions of the viscosity converted from Fig. 8 based on their relationship shown in Fig. 3 [50]. In the case of the nonreactive fluid pairs, even though the concentration in the finger continuously changed in the flow direction, the viscosity changed very sharply, which reflected the relationship between them, as shown in Fig. 3(b). Therefore, for this nonreactive fluid pair, the broad density profile due to mixing did not sharply relax the viscosity contrast. On the other hand, for the reactive fluid pair, a clear local peak in the viscosity appeared in the viscosity profiles in the interface between the LVL and MVL. Behind the peak, an unfavorable viscosity profile of increasing viscosity along the flow direction appears, but the smooth viscosity gradients win and calm VF down. After the peak, the viscosity profiles were in favorable conditions. The peak viscosity tended to increase with the decrease in Pe or $\dot{\gamma}$, but the unfavorable gradient in the viscosity in the reactive fluid pairs was mild compared with the nonreactive cases. The favorable viscosity profile after the peak and the moderate unfavorable profile behind the peak might result in the stabilization of the VF even for high viscosity ratio as shown in Fig. 5. In the case of the nonreactive fluid pairs, the higher unfavorable viscosity gradient with decreasing Pe resulted in earlier breakthrough, which displayed a shear-thinning property of the displaced fluid, as shown in Fig. 3(b) [14,15,32].

B. Decreasing-viscosity system

In this section, we present the experimental results for the SPA-HCl system, where the chemical reaction decreases the mixture viscosity SPA-NaI solutions without chemical reaction as the reference system.

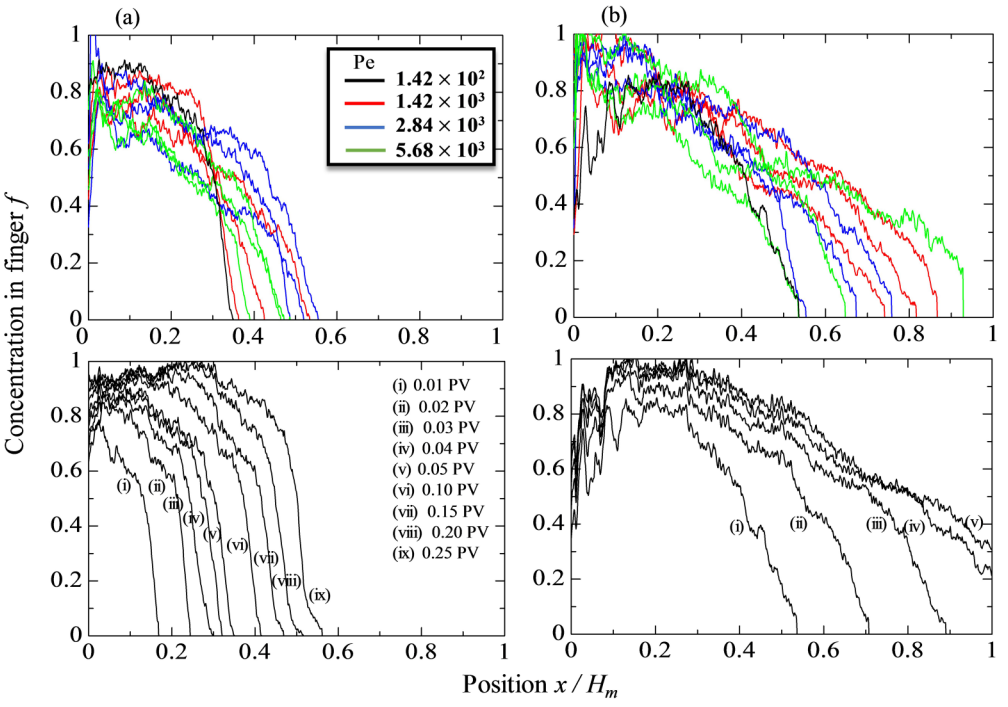

FIG. 8. Distribution of the normalized concentration of LVL $f = C_{\max}/C_0$ along the most advanced fingers for various Pe values for the (a) reactive (PAA-NaOH) and (b) nonreactive (PAA-NaI) cases. The figures at the top show the distribution of the normalized concentration after injection of 0.05 PV of LVL for high Pe values (1.42×10^3, 2.84×10^3, and 5.68×10^3). The figures at the bottom show the successive distribution after injection of (i) 0.01, (ii) 0.02, (iii) 0.03, (iv) 0.04, (v) 0.05, (vi) 0.10, (vii) 0.15, (viii) 0.20, and (ix) 0.25 PV for low Pe (1.42×10^2).

1. Effect of the Péclet number (Pe) on fingering

Figure 10 shows the 3D VF structure at various Pe values with and without a viscosity-decreasing chemical reaction after injection of 0.05 PV of LVL. Similar to that shown in Fig. 4, i.e., increasing-viscosity system, all fingers displayed an isocontour surface of the normalized NaI concentration, namely, LVL volume fraction $f = C/C_0 = 0.25$. For a reactive fluid pair, the tips of the fingers were located at a greater distance than that in the nonreactive fluid pair for all Pe values. For both reactive and nonreactive cases, the position of the most advanced finger decreased with increasing Pe because of the shear-thinning property of the SPA, in which the SPA viscosity, i.e., M, decreased with Pe.

2. Growth of fingers and distribution of local concentration and viscosity

Figures 11 and 12 show the evolution of 3D VF structure with time and the distribution of f and viscosity. Similar to that shown in Figs. 5 and 6, the local concentration of LVL f was estimated from the CT value using the correlation curves obtained from the preliminary experiments and then converted into viscosity using the relationship between f and the viscosity, as shown in Fig. 3 [50]. In the case of the chemical reaction with decreasing viscosity (Fig. 11), a single finger extended straight downward from the injection point, and one of the split fingers reached the exit with the injection of 0.05 PV. The concentration in the finger intensively decreased from the point of injection. Compared with the finger structure [Fig. 11(a)] where an isocontour surface of $f = C/C_0 = 0.25$ was shown, the region displayed reduced viscosity because the mixing of LVL

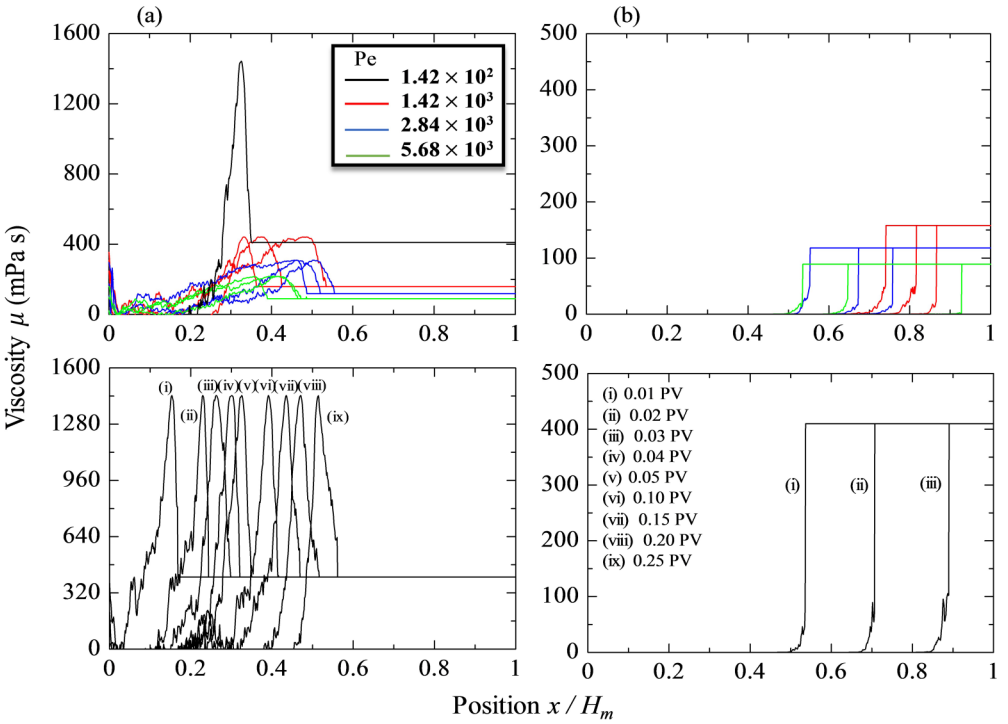

FIG. 9. Viscosity distribution along the most advanced finger for the (a) reactive (PAA-NaOH) and (b) nonreactive (PAA-NaI) cases. According to the relationship between the viscosity and LVL concentration, the concentration distribution shown in Fig. 8 is transformed into viscosity. The figures at the top show the viscosity distribution after injection of 0.05 PV of LVL for high Pe values (1.42×10^3, 2.84×10^3, and 5.68×10^3). The figures at the bottom show the successive distribution after injection of (i) 0.01, (ii) 0.02, (iii) 0.03, (iv) 0.04, (v) 0.05, (vi) 0.10, (vii) 0.15, (viii) 0.20, and (ix) 0.25 PV for low Pe (1.42×10^2).

and MVL broadly extended and some fingers that were not shown in Fig. 11(b) were observed in the viscosity map [Fig. 11(c)]. This fact suggested that some of the branched fingers vanished because of the intensive mixing of the LVL and MVL. In the nonreactive case (Fig. 12), more-active tip splitting occurred than in the reactive case.

3. Area fraction of injected LVL

The area fraction is defined as the ratio of the area of the finger when the concentration of the LVL is higher than $f = 0.25$ to the cross-sectional area of the packed bed, is shown in Fig. 13 under various Pe values. As discussed in the previous section, the fingers that grew with the reaction were thinner than those without reaction because of the decrease in the viscosity due to the chemical reaction. As a result, the area fraction of LVL in the reactive cases was lower than that in the nonreactive cases. The position of the tip of the most advanced finger decreased with increasing Pe for the reactive and the nonreactive case because of the shear-thinning property.

4. Distribution of concentration of LVL and viscosity along the most advanced fingering

Figure 14 shows the distribution of the local maximum LVL concentration within the most advanced finger for various Pe values. At the injection of 0.05 PV of LVL (Fig. 14, top), the concentration in the finger quickly reduced from the injection point ($x/H_m = 0$) down to approximately 0.5 in the reactive cases. In the nonreactive cases, the concentration mildly reduced

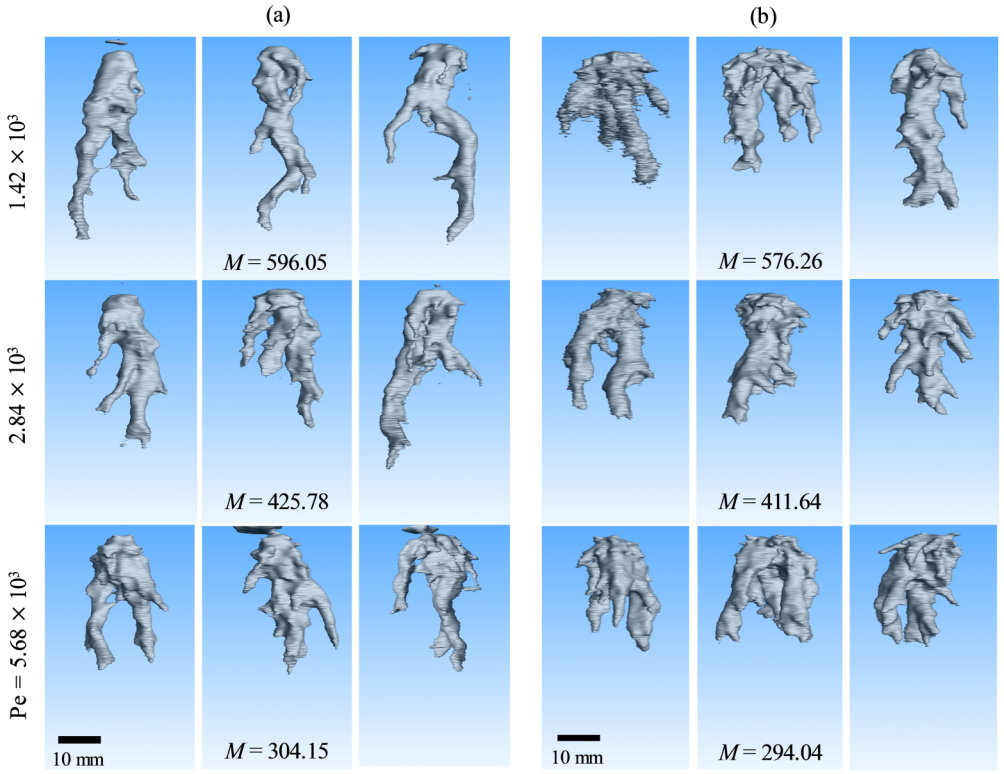

FIG. 10. 3D VF structure in the packed bed after injection of 0.05 PV of LVL for various Pe and M values for the (a) reactive (SPA-HCl) and (b) nonreactive (SPA-NaI) fluid pairs. The isocontour surface corresponds to the concentration of LVL, $f = C/C_0 = 0.25$. The three panels given for each M and Pe represent the results from three repeated experiments with the same experimental conditions.

to approximately 0.6 and then sharply decreased at the tip of the finger. At low Pe of 0.71×10^2 (Fig. 14, bottom), the tip of the finger advances with time, whereas in the finger, the concentration hardly recovered above 0.4 in the reactive case. This concentration profile reflected intensive fingering and mixing, as mentioned above. Figure 15 shows the viscosity profiles converted from Fig. 14 based on the relationship between f and the viscosity shown in Fig. 3. Displaying intensive mixing, the unfavorable viscosity gradient was mild in the reactive cases compared with that in the nonreactive cases.

C. Sweep efficiency

We defined sweep efficiency E as the ratio of the volume occupied by the injected LVL when $f > 0.25$ to the cylindrical domain with a height between the injection point and tip of the most advanced finger with the cross-sectional area of the packed bed at the injection of 0.05 PV of LVL. For the increasing-viscosity system [Fig. 16(a)], the sweep efficiency was higher in the reactive cases than that in the nonreactive cases regardless of Pe because the VF development in the reactive cases was suppressed by the increasing viscosity via a chemical reaction compared with that in the nonreactive cases as discussed above. For the decreasing-viscosity system, however, the sweep efficiency in the reactive cases was lower than that in the nonreactive cases because the fingers in the reactive cases were much narrower than those in the nonreactive cases, as shown in Fig. 9. Some large discrepancies in sweep efficiency in the nonreactive cases might be caused by the difference in fingering structure due to fluctuations of viscous fingering from each repeated experiment as shown

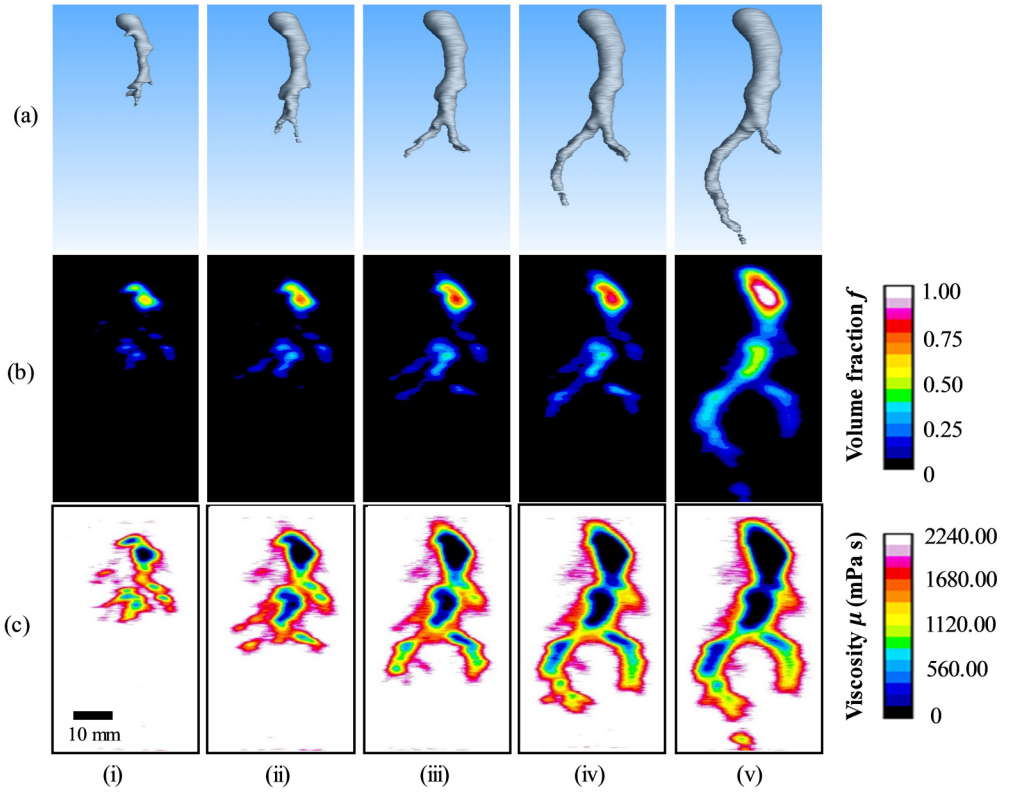

FIG. 11. Evolution of the (a) 3D structure of the fingers, (b) LVL concentration, and (c) viscosity with chemical reaction (SPA-HCl) at $\mathrm{Pe} = 0.71\times10^{2}$ and $M = 2608.65$ after injection of LVL with (i) 0.01, (ii) 0.02, (iii) 0.03, (iv) 0.04, and (v) 0.05 PV.

in Figs. 4 and 10. These results showed a good agreement with the Hele-Shaw cell experiments [32], which demonstrated that, for the increasing-viscosity system, the area density of the fingering with chemical reactions was larger than that without chemical reactions. The area density of the fingering with chemical reactions was inversely smaller than that without chemical reactions in the decreasing-viscosity system. As discussed in the previous section, the reactions and polymers used here are the same as in [32], in which the effect of reactions on VF was studied in Hele-Shaw cells. We emphasized that the fluids were not considered as Newtonian in [32]. The Hele-Shaw experiment was conducted under the condition of shear rate where the elastic property was able to be neglected. However, shear-thinning viscosity, one of the typical non-Newtonian properties, could be present in [32] as well as in the present study (3D cases) although it was not explicitly mentioned in [32]. The present results experimentally demonstrate that the influence of changes (increase or decrease) in viscosity induced by chemical reactions on the dynamics of miscible viscous fingering in a Hele-Shaw cell is maintained in 3D porous media. In addition, in the present study, a microfocused x-ray CT scanner enables us to examine distribution of concentration and viscosity in the fingering, which was not investigated in the Hele-Shaw experiment. The present study claimed that the property of shear-thinning viscosity worked in the VF dynamics; that is, VF in both the nonreactive cases developed more intensively and led to earlier breakthrough as Pe was larger because of the higher viscosity ratio at lower shear rate, which had originated from the shear-thinning viscosity of the displaced polymer fluids. We noted the property of shear-thinning viscosity could be present in [32] as well as in the present study (3D cases) although it was not explicitly mentioned in [32]. In fact, in Figs. 8 and 9 [32], the area density of the radial fingering denoted as d_a increased with an increase

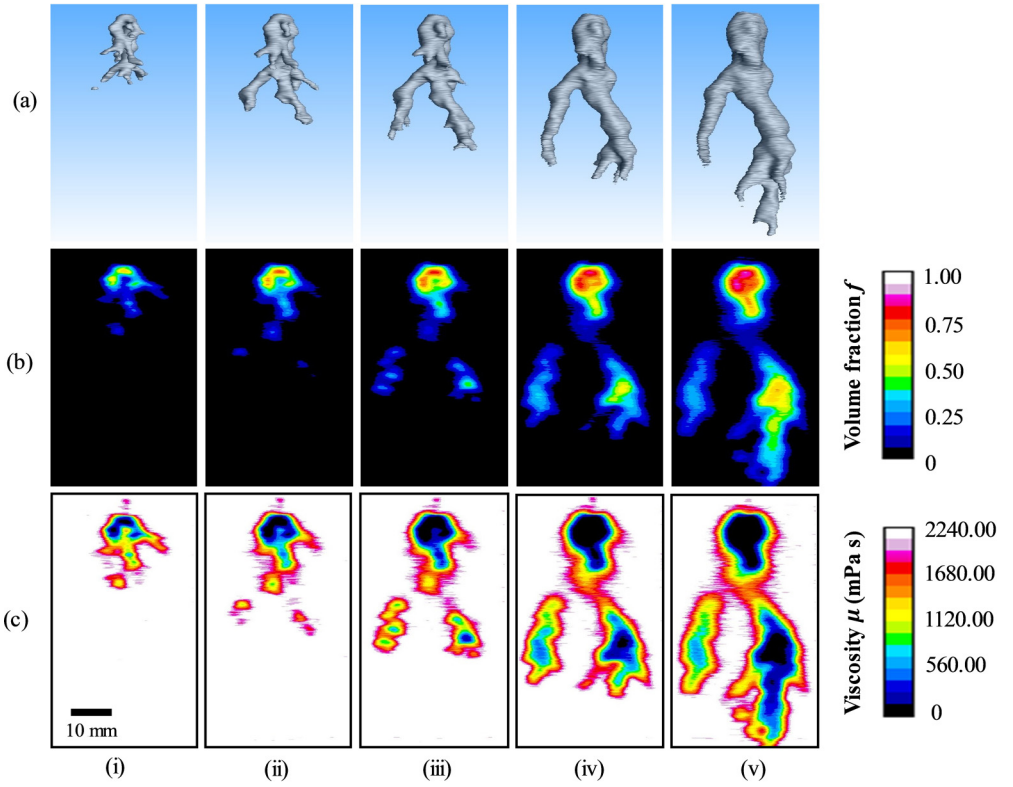

FIG. 12. Evolution of the (a) 3D structure of fingers, (b) LVL concentration, and (c) viscosity without chemical reaction (SPA-NaI) at $\mathrm{Pe} = 0.71 \times 10^2$ and $M = 2522.02$ after injection of LVL with (i) 0.01, (ii) 0.02, (iii) 0.03, (iv) 0.05, and (v) 0.07 PV.

in the flow rate represented by Pe_v in both the nonreactive systems. If the fluids were Newtonian, d_a would decrease with an increase in Pe_v due to a more-unstable situation. However, Figs. 8 and 9 [32] showed the opposite results, which are considered to be caused by the shear-thinning viscosity; with an increase in Pe_v, the displaced fluid's viscosity was smaller due to shear-thinning viscosity,

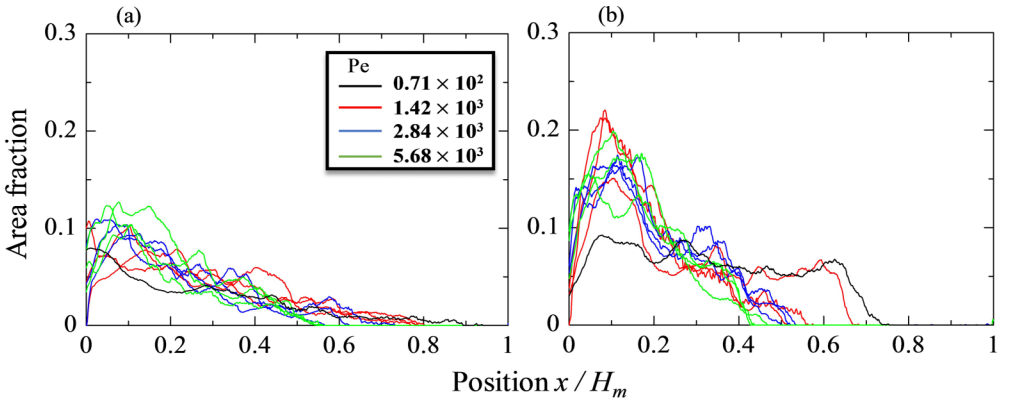

FIG. 13. Area fraction of the LVL for various Pe values after injection of 0.05 PV of LVL for the (a) reactive (SPA-HCl) and (b) nonreactive (SPA-NaI) fluid systems.

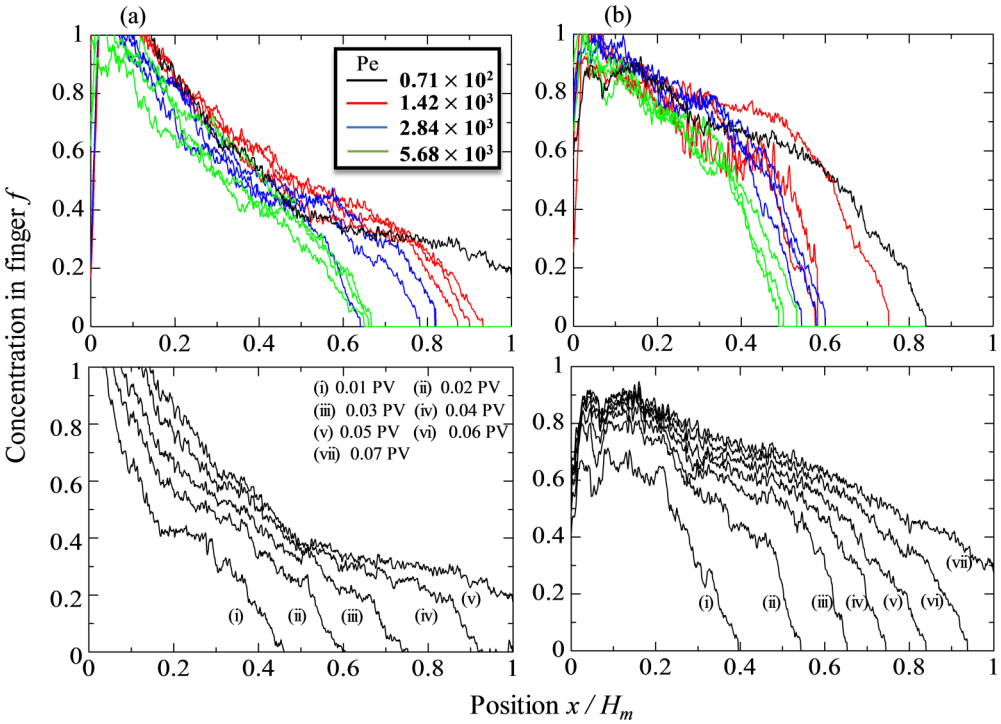

FIG. 14. Distribution of the normalized concentration of LVL $f = C_{\max}/C_0$ along the most advanced fingers for various Pe values for the (a) reactive (SPA-HCl) and (b) nonreactive (SPA-NaI) cases. The figures at the top show the distribution of the normalized concentration after injection of 0.05 PV of LVL for high Pe values (1.42×10^3, 2.84×10^3, and 5.68×10^3). The figures at the bottom show the successive distribution after injection of (i) 0.01, (ii) 0.02, (iii) 0.03, (iv) 0.04, (v) 0.05, (vi) 0.06, and (vii) 0.07 PV for low Pe (0.71×10^2).

leading to smaller viscosity contrast, which resulted in a less-unstable situation. In the present study, we have explicitly mentioned such a phenomenon: VF in both the nonreactive cases developed more intensively and led to earlier breakthrough as Pe was larger because of the higher viscosity ratio at lower shear rate, which had originated from the shear-thinning viscosity of the displaced polymer fluids.

IV. CONCLUSIONS

The 3D VF structure in porous media for miscible non-Newtonian fluids with chemical reaction has been successfully visualized using a microfocus x-ray CT scanner. We employed the PAA-NaOH and SPA-HCl systems as non-Newtonian fluids in which the viscosity increased and decreased, respectively, with the chemical reaction.

For the increasing-viscosity system (PAA-NaOH), VF was induced around the spot-injection point, and the fingers extended downward both with and without the chemical reaction. In the case of the reactive fluids, the length of the fingers was shorter than that in the nonreactive cases where several long and thick fingers developed. At low Pe of 1.42×10^2, pistonlike displacement occurred in the packed bed, except for the region near the tube wall. Immediately after the injection started, VF could develop because a displacement front with a hemispherical shape developed, which was centered at the point of injection. However, the tips of the fingers were influenced by the tube wall, the fingers merged with one another, and a thick viscous layer was formed, which surrounded the LVL. The cylindrical domain of the displacing LVL was surrounded by a high-viscosity

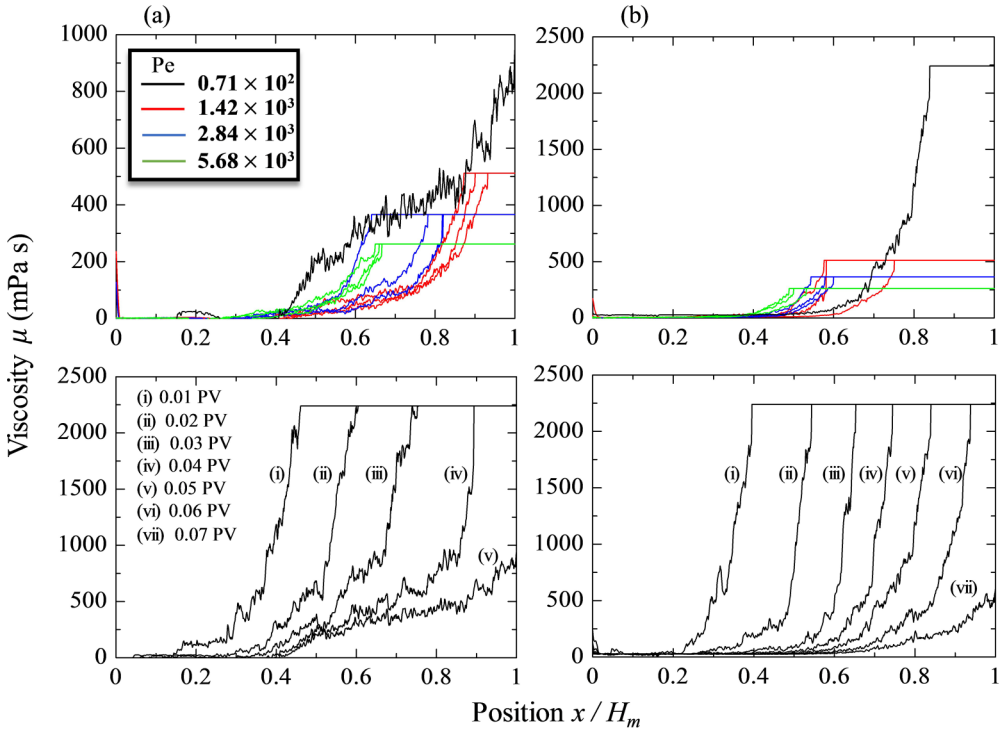

FIG. 15. Viscosity distribution along the most advanced finger for the (a) reactive (SPA-HCl) and (b) nonreactive (SPA-NaI) cases. According to the relationship between the viscosity and LVL concentration, the concentration distribution shown in Fig. 14 is transformed into viscosity. The figures at the top show the viscosity distribution after injection of 0.05 PV of LVL for high Pe values (1.42×10^3, 2.84×10^3, and 5.68×10^3). The figures at the bottom show the successive distribution after injection of (i) 0.01, (ii) 0.02, (iii) 0.03, (iv) 0.04, (v) 0.05, (vi) 0.06, and (vii) 0.07 PV for low Pe (0.71×10^2).

filmlike layer because of the chemical reaction, which impeded the mixing of the LVL and MVL. Consequently, inside this layer, a high concentration of LVL was maintained without mixing with the MVL. As a result, the fingering development was impeded, and the breakthrough was delayed. In the nonreactive case, however, VF intensively developed and led to early breakthrough because of the high viscosity ratio at low shear rate. These results were consistent with the experimental and theoretical research works of shear-thinning fluids in a Hele-Shaw cell [14,15,18]. In the case of the reactive fluid pair, the profiles of the area fraction resembled each other for all Pe values and the effect of Pe as well as M was not clear because of the suppression of VF. In the nonreactive case the tip of the fingers further advanced compared with that in the reactive case and went further with the decrease in Pe, namely, with the increase in M, which reflected the property of shear-thinning fluids. In the case of the nonreactive fluid pairs, even though the local concentration of LVL in the finger continuously changed in the flow direction, the viscosity very sharply changed. Therefore, the broad density profile due to mixing did not sharply relax the viscosity contrast. On the other hand, for the reactive fluid pair, a clear local peak in the viscosity appeared in the viscosity profiles in the interface between the LVL and MVL. The smooth viscosity gradients appeared along the flow direction behind the peak of the viscosity profile that overcame the VF although it was in the unfavorable conditions. After the peak, the viscosity profiles were in favorable conditions.

By contrast, in the decreasing-viscosity system (SPA-HCl), for the reactive fluid pair, the tips of the fingers were located at greater distance than those in the nonreactive fluid pair for all Pe values.

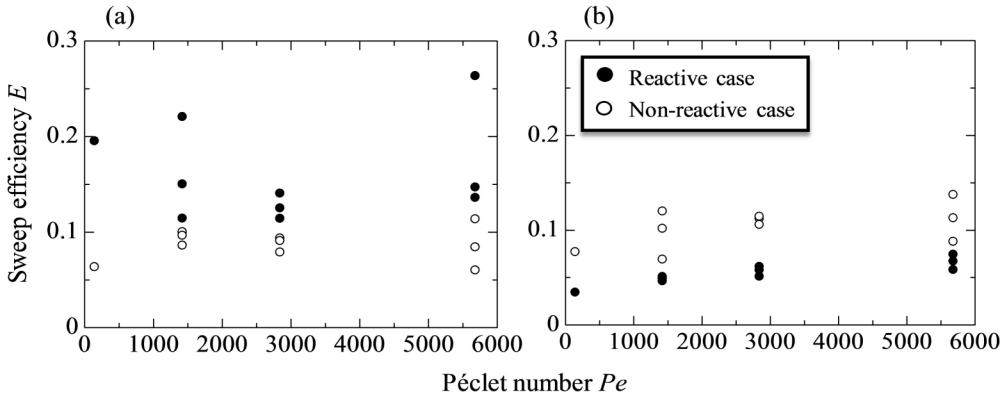

FIG. 16. Sweep efficiency for the (a) increasing-viscosity and (b) decreasing-viscosity systems. Three points in the reactive and nonreactive cases for each Pe represent the results from three repeated experiments with the same experimental conditions.

For both reactive and nonreactive cases, the position of the most advanced finger decreased with increasing Pe, because of the shear-thinning property of SPA. At low Pe of 0.71×10^2, in the case of the chemical reaction, a single finger extended straight downward from the injection point, and one of the split fingers reached the exit with the injection of 0.05 PV. The concentration in the finger intensively reduced from the point of injection because of the intensive mixing of the LVL and MVL. As a result, the area fraction of injected LVL in the reactive cases was lower than that in the nonreactive cases for all Pe values. In the nonreactive case, more-active tip splitting occurred than in the reactive case. The position of the tip of the most advanced finger decreased with increasing Pe for the reactive and nonreactive case, because of the shear-thinning property. In the reactive cases, the LVL concentration in the finger quickly decreased from the injection point down to $f = 0.5$. In the nonreactive cases, the concentration mildly decreased down to approximately 0.6 and then sharply decreased at the tip of the finger. At low Pe of 0.71×10^2, the tip of the finger advanced with time, whereas in the finger, the concentration of LVL hardly recovered above 0.4 in the reactive case. This concentration profile reflects intensive fingering and mixing.

ACKNOWLEDGMENT

This work was supported by the JSPS KAKENHI Grant No. 17H00790.

[1] G. M. Homsy, Viscous fingering in porous media, Annu. Rev. Fluid Mech. **19**, 271 (1987).
[2] A. De Wit, Y. Bertho, and M. Martin, Viscous fingering of miscible slices, Phys. Fluids **17**, 054114 (2005).
[3] T. Suekane, J. Ono, A. Hyodo, and Y. Nagatsu, Three-dimensional viscous fingering of miscible fluids in porous media, Phys. Rev. Fluids **2**, 103902 (2017).
[4] L. W. Lake, R. L. Schmidt, and P. B. Venuto, A niche for enhanced oil recovery in the 1990s, Oilfield Rev. **4**, 55 (1992).
[5] A. Buka, P. Palffy-Muhoray, and Z. Racz, Viscous fingering in liquid crystals, Phys. Rev. A **36**, 3984 (1987).
[6] M. L. Dickson, T. T. Norton, and E. J. Fernandez, Chemical imaging of multicomponent viscous fingering in chromatography, AIChE J. **43**, 409 (1997).
[7] D. H. Vlad and J. V. Maher, Tip-splitting instabilities in the channel Saffman-Taylor flow of constant viscosity elastic fluids, Phys. Rev. E **61**, 5439 (2000).

[8] S. Hill, Channeling in packed columns, Chem. Eng. Sci. **1**, 247 (1952).
[9] L. A. Riolfo, Y. Nagatsu, P. M. J. Trevelyan, and A. De Wit, Chemically-driven miscible viscous fingering: How can a reaction destabilize typically stable fluid displacements?, in *Proceedings of the European Conference on Complex Systems, Springer Proceeding in Complexity* (Springer, Berlin, 2012), p. 9.
[10] D. Bensimon, L. P. Kadanoff, S. Liang, B. I. Shraiman, and C. Tang, Viscous flows in two dimensions, Rev. Mod. Phys. **58**, 977 (1986).
[11] Y. C. Yortsos, Instabilities in displacement processes in porous media, J. Phys.: Condens. Matter **2**, SA443 (1990).
[12] J. C. Bacri, D. Salin, and R. Wouméni, Three-Dimensional Miscible Viscous Fingering in Porous Media, Phys. Rev. Lett. **67**, 2005 (1991).
[13] J. Nittmann, G. Daccord, and H. E. Stanley, Fractal growth of viscous fingers: Quantitative characterization of a fluid instability phenomenon, Nature **314**, 141 (1985).
[14] A. Lindner, D. Bonn, E. C. Poiré, M. Ben Amar, and J. Meunier, Viscous fingering in non-Newtonian fluids, J. Fluid Mech. **469**, 237 (2002).
[15] A. Lindner, D. Bonn, and J. Meunier, Viscous fingering in a shear-thinning fluid, Phys. Fluids **12**, 56 (2000).
[16] D. Bonn and J. Meunier, Viscoelastic Free-Boundary Problems: Non-Newtonian Viscosity vs Normal Stress Effects, Phys. Rev. Lett. **79**, 2662 (1997).
[17] G. Daccord, J. Nittmann, and H. E. Stanley, Radial Viscous Fingers and Diffusion-Limited Aggregation: Fractal Dimension and Growth Sites, Phys. Rev. Lett. **56**, 336 (1986).
[18] J. E. Sader, D. Y. C. Chan, and B. D. Hughes, Non-Newtonian effects on immiscible viscous fingering in a radial Hele-Shaw cell, Phys. Rev. E **49**, 420 (1994).
[19] T. Yamamoto, H. K. Amikawa, H. T. Anaka, K. N. Akamura, and N. M. Ori, Viscous fingering of non-Newtonian fluids in a rectangular Hele-Shaw cell, Nihon Reoroji Gakkaishi **29**, 81 (2001).
[20] J. Fernandez and G. M. Homsy, Viscous fingering with chemical reaction: Effect of in-situ production of surfactants, J. Fluid Mech. **480**, 267 (2003).
[21] M. Jahoda and V. Hornof, Concentration profiles of reactant in a viscous finger formed during the interfacially reactive immiscible displacements in porous media, Powder Technol. **110**, 253 (2000).
[22] V. Hornof and F. U. Baig, Influence of interfacial reaction and mobility ratio on the displacement of oil, Exp. Fluids **18**, 448 (1995).
[23] V. Hornof and C. Bernard, Effect of interfacial reaction on immiscible displacement in Hele-Shaw cells, Exp. Fluids **12**, 425 (1992).
[24] V. Hornof, G. H. Neale, and M. G. Hosseini, Effects of flow rate and alkali-to-acid ratio on the displacement of acidic oil by alkaline solutions in radial porous media, J. Colloid Interface Sci. **231**, 196 (2000).
[25] Y. Nagatsu, Y. Ishii, Y. Yada, and A. De Wit, Hydrodynamic Fingering Instability Induced by a Precipitation Reaction, Phys. Rev. Lett. **113**, 024502 (2014).
[26] Y. Nagatsu, S.-K. Bae, Y. Kato, and Y. Tada, Miscible viscous fingering with a chemical reaction involving precipitation, Phys. Rev. E **77**, 067302 (2008).
[27] F. Haudin and A. De Wit, Patterns due to an interplay between viscous and precipitation-driven fingering, Phys. Fluid. **27**, 113101 (2015).
[28] A. De Wit and G. M. Homsy, Nonlinear interactions of chemical reactions and viscous fingering in porous media, Phys. Fluids **11**, 949 (1999).
[29] S. H. Hejazi, P. M. J. Travelyan, J. Azaiez, and A. De Wit, Viscous fingering of a miscible reactive $A + B \rightarrow C$ interface: A linear stability analysis, J. Fluid Mech. **652**, 501 (2010).
[30] Y. Nagatsu and A. De Wit, Viscous fingering of a miscible reactive $A + B \rightarrow C$ interface for an infinitely fast chemical reaction: Nonlinear simulations, Phys. Fluids **23**, 043103 (2011).
[31] S. Stewart, D. Marin, M. Tullier, J. Pojman, E. Meiburg, and P. Bunton, Stabilization of miscible viscous fingering by a step growth polymerization reaction, Exp. Fluids **59**, 114 (2018).
[32] Y. Nagatsu, K. Matsuda, Y. Kato, and Y. Tada, Experimental study on miscible viscous fingering involving viscosity changes induced by variations in chemical species concentrations due to chemical reactions, J. Fluid Mech. **571**, 475 (2007).

[33] L. A. Riolfo, Y. Nagatsu, S. Iwata, R. Maes, P. M. J. Trevelyan, and A. De Wit, Experimental evidence of reaction-driven miscible viscous fingering, Phys. Rev. E **85**, 015304(R) (2012).
[34] Y. Nagatsu, C. Iguchi, K. Matsuda, Y. Kato, and Y. Tada, Miscible viscous fingering involving viscosity changes of the displacing fluid by chemical reactions, Phys. Fluids **22**, 024101 (2010).
[35] T. Gérard and A. De Wit, Miscible viscous fingering induced by a simple A + B → C chemical reaction, Phys. Rev. E **79**, 016308 (2009).
[36] Y. Nagatsu, Y. Kondo, Y. Kato, and Y. Tada, Effects of moderate Damköhler number on miscible viscous fingering involving viscosity decrease due to a chemical reaction, J. Fluid Mech. **625**, 97 (2009).
[37] A. De Wit and G. M. Homsy, Viscous fingering in reaction-diffusion systems, J. Chem. Phys. **110**, 8663 (1999).
[38] Y. Nagatsu, Y. Kondo, Y. Kato, and Y. Tada, Miscible viscous fingering involving viscosity increase by a chemical reaction with moderate Damköhler number, Phys. Fluids **23**, 014109 (2011).
[39] S. H. Hejazi and J. Azaiez, Non-linear interactions of dynamic reactive interfaces in porous media, Chem. Eng. Sci. **65**, 938 (2010).
[40] M. Z. Saghir, O. Chaalal, and M. R. Islam, Numerical and experimental modeling of viscous fingering during liquid-liquid miscible displacement, J. Pet. Sci. Eng. **26**, 253 (2000).
[41] H. R. Zhang, K. S. Sorbie, and N. B. Tsibuklis, Viscous fingering in five-spot experimental porous media: New experimental results and numerical simulation, Chem. Eng. Sci. **52**, 1 (1997).
[42] L. Paterson, Fingering with miscible fluids in a Hele Shaw cell, Phys. Fluids **28**, 26 (1985).
[43] P. Petitjeans, C. Y. Chen, E. Meiburg, and T. Maxworthy, Miscible quarter five-spot displacements in a Hele-Shaw cell and the role of flow-induced dispersion, Phys. Fluids **11**, 1705 (1999).
[44] C. Jiao and T. Maxworthy, An experimental study of miscible displacement with gravity-override and viscosity-contrast in a Hele Shaw cell, Exp. Fluids **44**, 781 (2008).
[45] R. Metzner, A. Eggert, D. V. Dusschoten, D. Pflugfelder, S. Gerth, U. Schurr, N. Uhlmann, and S. Jahnke, Direct comparison of MRI and x-ray CT technologies for 3D imaging of root systems in soil: Potential and challenges for root trait quantification, Plant Methods **11**, 17 (2015).
[46] E. Herremans, A. Melado-Herreros, T. Defraeye, B. Verlinden, M. Hertog, P. Verboven, J. Val, M. E. Fernández-Valle, E. Bongaers, P. Estrade, M. Wevers, P. Barreiro, and B. M. Nicolaï, Postharvest biology and technology comparison of x-ray CT and MRI of watercore disorder of different apple cultivars, Postharvest Biol. Technol. **87**, 42 (2014).
[47] H. E. L. Rose and M. M. Britton, Microporous and mesoporous materials magnetic resonance imaging of reaction-driven viscous fingering in a packed bed, Microporous Mesoporous Mater. **178**, 64 (2013).
[48] R. A. Ketcham and W. D. Carlson, Acquisition, optimization and interpretation of x-ray computed tomographic imagery: Applications to the geosciences, Comput. Geosci. **27**, 381 (2001).
[49] A. Patmonoaji and T. Suekane, Advances in water resources investigation of CO_2 dissolution via mass transfer inside a porous medium, Adv. Water Resour. **110**, 97 (2017).
[50] See Supplemental Material at http://link.aps.org/supplemental/10.1103/PhysRevFluids.4.054502 for concentration and viscosity calibration curves, parameter determined from rheological data and videos of runs PAA-NaOH (Fig. 5), PAA-NaI (Fig. 6), SPA-HCl (Fig. 11), and SPA-NaI (Fig. 12).